Available online at www.sciencedirect.com
SCIENCE DIRECT®
ELSEVIER
International Journal of Solids and Structures 43 (2006) 2193–2208
INTERNATIONAL JOURNAL OF SOLIDS and STRUCTURES
www.elsevier.com/locate/ijsolstr

Two new expanding cavity models for indentation deformations of elastic strain-hardening materials

X.-L. Gao [a,*], X.N. Jing [b], G. Subhash [b]

[a] *Department of Mechanical Engineering, Texas A&M University, 3123 TAMU, College Station, TX 77843-3123, USA*
[b] *Department of Mechanical Engineering-Engineering Mechanics, Michigan Technological University, 1400 Townsend Drive, Houghton, MI 49931-1295, USA*

Received 22 December 2004; received in revised form 21 March 2005
Available online 23 May 2005

Abstract

Two expanding cavity models (ECMs) are developed for describing indentation deformations of elastic power-law hardening and elastic linear-hardening materials. The derivations are based on two elastic–plastic solutions for internally pressurized thick-walled spherical shells of strain-hardening materials. Closed-form formulas are provided for both conical and spherical indentations, which explicitly show that for a given indenter geometry indentation hardness depends on Young's modulus, yield stress and strain-hardening index of the indented material. The two new models reduce to Johnson's ECM for elastic-perfectly plastic materials when the strain-hardening effect is not considered. The sample numerical results obtained using the two newly developed models reveal that the indentation hardness increases with the Young's modulus and strain-hardening level of the indented material. For conical indentations the values of the indentation hardness are found to depend on the sharpness of the indenter: the sharper the indenter, the larger the hardness. For spherical indentations it is shown that the hardness is significantly affected by the strain-hardening level when the indented material is stiff (i.e., with a large ratio of Young's modulus to yield stress) and/or the indentation depth is large. When the indentation depth is small such that little or no plastic deformation is induced by the spherical indenter, the hardness appears to be independent of the strain-hardening level. These predicted trends for spherical indentations are in fairly good agreement with the recent finite element results of Park and Pharr.

Keywords: Indentation; Hardness; Expanding cavity model; Conical indenter; Spherical indenter; Power-law hardening; Linear hardening; Elastic–plastic material

* Corresponding author. Tel.: +1 979 845 4835; fax: +1 979 845 3081.
E-mail address: xlgao@tamu.edu (X.-L. Gao).

0020-7683/$ - see front matter © 2005 Elsevier Ltd. All rights reserved.
doi:10.1016/j.ijsolstr.2005.03.062

1. Introduction

Indentation tests have been widely used to measure hardness and other material properties including Young's modulus, yield stress and strain-hardening index (e.g., Tabor, 1951, 1986; Fischer-Cripps, 2002; Wei and Hutchinson, 2003; Cheng and Cheng, 2004). The indentation hardness can be determined as the ratio of applied load to projected area of the indentation, both of which are measured in indentation tests. For rigid-perfectly plastic materials, it is known that the indentation hardness H is directly related to the yield stress σ_y through $H = 3\sigma_y$, which is obtained from the slip line field theory (e.g., Tabor, 1951). Based on Hill's (1950) solution for the quasi-static expansion of an internally pressurized spherical shell of an elastic-perfectly plastic material, expanding cavity models (ECMs) have been developed (Marsh, 1964; Hirst and Howse, 1969; Johnson, 1970) to describe indentation responses of various materials.

In Johnson's ECM (Johnson, 1970), the indenter was assumed to be encapsulated by a hemispherical hydrostatic core. For conical indentations, the ECM based on the von Mises yield criterion and material incompressibility assumption predicts (Johnson, 1970)

$$\frac{H}{\sigma_y} = \frac{2}{3}\left[1 + \ln\left(\frac{1}{3}\frac{E}{\sigma_y}\cot\alpha\right)\right], \tag{1}$$

where H, σ_y and E are, respectively, the hardness, yield stress and Young's modulus of the indented material, and α is the half included (or cone) angle of a conical indenter.

Because of their simplicity and predictability, the expanding cavity models (ECMs) developed using solutions for elastic-perfectly plastic shells have been frequently used to characterize indentation deformations. For example, an ECM based on the Drucker–Prager yield criterion was recently employed to study indentation responses of pressure sensitive, elastic-perfectly plastic solids to conical and spherical indentations (Narasimhan, 2004). However, such expanding cavity models have been found to break down for materials having appreciable strain-hardening characteristics (e.g., Tabor, 1986; Lawn, 1998). As a result, finite element simulations have been used to study indentation deformations of strain-hardening materials induced by a sharp indenter (e.g., Giannakopoulos and Suresh, 1999; Zhang and Subhash, 2001; Mata et al., 2002; Mata and Alcala, 2003) or by a spherical indenter (e.g., Fischer-Cripps, 1997; Mesarovic and Fleck, 1999; Park and Pharr, 2004). Nevertheless, no analytical formula has been derived for determining hardness of a strain-hardening material. Therefore, new elastic–plastic ECMs that are capable of incorporating the strain-hardening effect on indentation deformations are still in need.

The objective of the current study is to develop two of such new models for describing conical and spherical indentations of elastic power-law hardening and elastic linear-hardening materials, respectively. The rest of this paper is organized as follows. In Section 2, the solutions for internally pressurized spherical shells of both elastic power-law hardening and elastic linear-hardening materials are presented. This is followed by the development of the two new ECMs in Section 3, which analytically incorporates the strain-hardening characteristics of materials for the first time. It is shown that the new ECMs can be reduced to Johnson's ECM for elastic-perfectly plastic materials when the strain-hardening effect is ignored. In Section 4, the newly developed ECMs are directly applied to conduct a parametric study, where the numerical data predicted by the new ECMs are also compared to existing finite element results. The paper concludes with a summary in the fifth and last section.

2. Solutions for internally pressurized spherical shells of strain-hardening materials

In this section, the stress, strain and displacement components in a thick-walled spherical shell of the inner radius r_i and outer radius r_o subjected to the internal pressure p_i are presented.

For linearly elastic, power-law hardening plastic materials, the stress–strain relation can be represented by (e.g., Gao and Wei, 1991; Gao, 1992)

$$\sigma_e = \begin{cases} E\varepsilon_e & (\sigma_e \leqslant \sigma_y) \\ k\varepsilon_e^n & (\sigma_e > \sigma_y) \end{cases}, \tag{2}$$

where σ_e and ε_e are, respectively, the effective stress and the effective strain, n is the strain-hardening exponent ($0 \leqslant n \leqslant 1$), and k is a material constant related to the yield stress (σ_y) and Young's modulus (E) by $k = E^n/\sigma_y^{n-1}$. When $n = 0$, Eq. (2) recovers the stress–strain relation of elastic-perfectly plastic materials, and when $n = 1$, Eq. (2) reduces to the Hooke's law for linearly elastic materials.

For elastic, linear-hardening plastic materials, the stress–strain relation can be represented by (e.g., Gao, 1993, 1994)

$$\sigma_e = \begin{cases} E\varepsilon_e & (\sigma_e \leqslant \sigma_y) \\ \sigma_y + E_p(\varepsilon_e - \varepsilon_y) & (\sigma_e > \sigma_y) \end{cases}, \tag{3}$$

where E_p is the tangent modulus, and ε_y is the yield strain satisfying $\varepsilon_y = \sigma_y/E$. When $E_p = 0$, Eq. (3) recovers the stress–strain relation for elastic-perfectly plastic materials, and when $E_p = E$, Eq. (3) reduces to the Hooke's law for linearly elastic materials.

The stress and displacement components in an internally pressurized spherical shell of the elastic power-law hardening material defined by Eq. (2) have been derived by Gao and Wei (1991) using Hencky's deformation theory, von Mises' yield criterion and the material incompressibility assumption. The solution of Gao and Wei (1991) (see also Gao, 2003) gives the stress, strain and displacement components in the plastic region ($r_i \leqslant r \leqslant r_c$) of the shell wall as

$$\begin{aligned}
\sigma_{rr} &= \frac{2}{3}\sigma_y\left[\left(\frac{1}{n} - 1\right) - \frac{1}{n}\left(\frac{r_c}{r}\right)^{3n} + \frac{r_c^3}{r_o^3}\right], \\
\sigma_{\theta\theta} &= \sigma_{\varphi\varphi} = \frac{2}{3}\sigma_y\left[\left(\frac{1}{n} - 1\right) + \left(\frac{3}{2} - \frac{1}{n}\right)\left(\frac{r_c}{r}\right)^{3n} + \frac{r_c^3}{r_o^3}\right], \\
\varepsilon_{rr} &= -\frac{\sigma_y}{E}\frac{r_c^3}{r^3}, \\
\varepsilon_{\theta\theta} &= \varepsilon_{\varphi\varphi} = \frac{\sigma_y}{2E}\frac{r_c^3}{r^3}, \\
u &= \frac{\sigma_y}{2E}\frac{r_c^3}{r^2},
\end{aligned} \tag{4a–e}$$

where r, θ, φ denote the coordinates in the spherical coordinate system, and r_c is the radius of the elastic–plastic interface that is related to the internal pressure p_i through

$$\frac{p_i}{\sigma_y} = \frac{2}{3}\left[\left(1 - \frac{r_c^3}{r_o^3}\right) + \frac{1}{n}\left(\frac{r_c^{3n}}{r_i^{3n}} - 1\right)\right]. \tag{5}$$

The stress components in the elastic region ($r_c \leqslant r \leqslant r_o$) of the shell wall are given by (Gao and Wei, 1991)

$$\sigma_{rr} = \frac{2\sigma_y}{3}\frac{r_c^3}{r_o^3}\left(1 - \frac{r_o^3}{r^3}\right), \quad \sigma_{\theta\theta} = \sigma_{\varphi\varphi} = \frac{2\sigma_y}{3}\frac{r_c^3}{r_o^3}\left(1 + \frac{r_o^3}{2r^3}\right), \tag{6a, b}$$

and the strain and displacement components in the elastic region have the same expressions as those listed in Eqs. (4c–e) for the plastic region.

Lamé's solution for a linearly elastic thick-walled spherical shell and Hill's solution for an elastic-perfectly plastic shell, both under an internal pressure, are included in the above solution as two limiting

cases with $n = 1$ and $n = 0$, respectively, as was shown in Gao and Wei (1991). In addition, the quasi-static expansion of a (small) spherical cavity in a very large medium of the elastic power-law hardening material can be described by using the solution of Gao and Wei (1991) with $r_o \to \infty$. For this particular case, the solution gives, letting $r_o \to \infty$ in Eq. (5),

$$\frac{p_i}{\sigma_y} = \frac{2}{3}\left\{1 + \frac{1}{n}\left[\left(\frac{r_c}{r_i}\right)^{3n} - 1\right]\right\}, \tag{7}$$

which will be directly employed to develop a new ECM for elastic power-law hardening materials in the next section.

The solution in the plastic region ($r_i \leqslant r \leqslant r_c$) of an internally pressurized spherical shell of the elastic linear-hardening plastic material defined by Eq. (3) is obtained as (see Appendix A)

$$\begin{aligned}
\sigma_{rr} &= \frac{2\sigma_y}{3}\left[-\left(1 - \frac{r_c^3}{r_o^3}\right) + \frac{E_p}{E}\left(1 - \frac{r_c^3}{r^3}\right) - 3\left(1 - \frac{E_p}{E}\right)\ln\frac{r_c}{r}\right],\\
\sigma_{\theta\theta} &= \sigma_{\varphi\varphi} = \frac{\sigma_y}{3}\left[1 + \frac{2r_c^3}{r_o^3} - \frac{E_p}{E}\left(1 - \frac{r_c^3}{r^3}\right) - 6\left(1 - \frac{E_p}{E}\right)\ln\frac{r_c}{r}\right],\\
\varepsilon_{rr} &= -\frac{\sigma_y}{E}\frac{r_c^3}{r^3},\\
\varepsilon_{\theta\theta} &= \varepsilon_{\varphi\varphi} = \frac{\sigma_y}{2E}\frac{r_c^3}{r^3},\\
u &= \frac{\sigma_y}{2E}\frac{r_c^3}{r^2},
\end{aligned} \tag{8a–e}$$

where r_c is defined by

$$\frac{p_i}{\sigma_y} = \frac{2}{3}\left[\left(1 - \frac{r_c^3}{r_o^3}\right) + \frac{E_p}{E}\left(\frac{r_c^3}{r_i^3} - 1\right)\right] + 2\left(1 - \frac{E_p}{E}\right)\ln\frac{r_c}{r_i}. \tag{9}$$

Notice that the strain and displacement components in the plastic region ($r_i \leqslant r \leqslant r_c$) here have the same expressions as those listed in Eqs. (4c–e) except that r_c involved in the expressions is now defined by Eq. (9) (rather than Eq. (5)).

Once again, Lamé's solution for a linearly elastic thick-walled spherical shell and Hill's solution for an elastic-perfectly plastic shell, both internally pressurized, can be recovered from the solution listed in Eqs. (8a–e) and (9) as two specific cases with $E_p/E = 1$ and $E_p/E = 0$, respectively. Also, the quasi-static expansion of a (small) spherical cavity in a very large medium of the elastic linear-hardening material can be described by using the afore-mentioned solution with $r_o \to \infty$. For this case, the solution gives, letting $r_o \to \infty$ in Eq. (9),

$$\frac{p_i}{\sigma_y} = \frac{2}{3}\left\{1 + \frac{E_p}{E}\left[\left(\frac{r_c}{r_i}\right)^3 - 1\right]\right\} + 2\left(1 - \frac{E_p}{E}\right)\ln\frac{r_c}{r_i}, \tag{10}$$

which will be directly used in the next section to develop a new ECM for elastic linear-hardening materials.

3. Expanding cavity models for elastic strain-hardening materials

In the expanding cavity model for elastic-perfectly plastic materials developed by Johnson (1970) based on the earlier studies of Marsh (1964) and Hirst and Howse (1969), the indentation process is idealized by encasing the contacting surface of the indenter in a hemispherical hydrostatic core of the radius a, which is

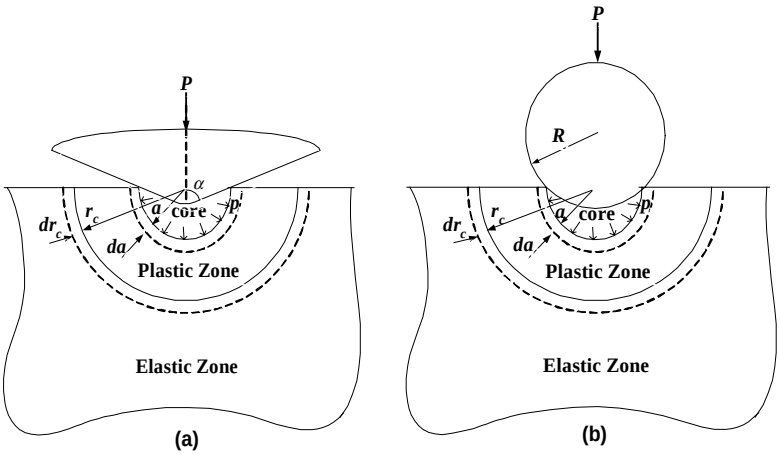

Fig. 1. Schematic of (a) conical indentation (b) spherical indentation with hydrostatic core radius a and plastic zone outer radius r_c.

surrounded by an incompressible hemispherical plastic zone of the outer radius r_c (see Fig. 1). This plastic zone is, in turn, constrained by an elastic region. An increment of penetration of the indenter is accompanied by a radial displacement of the core in the amount of da. The volume displaced by the movement of the indenter (and thus of the core) is accommodated by a radial expansion (dr_c) of the plastic zone and is eventually taken up by the elastic region. The pressure acting on the interface between the hydrostatic core and the plastic zone is taken to be equal to the mean indentation pressure, thereby measuring the hardness. This model is based on the experimentally observed fact (e.g., Marsh, 1964; Hirst and Howse, 1969) that the plastic zone beneath a Brinell-ball indenter or a blunt Vickers-pyramidal/conical indenter penetrating with the increase of applied load exhibits spherical symmetry, which resembles the plastic region near an expanding spherical cavity in an elastic–plastic solid. Subsequently, Hill's (1950) solution for the expansion of a spherical shell of an elastic-perfectly plastic material under an internal pressure was adopted in developing the afore-mentioned expanding cavity model.

To develop ECMs for elastic strain-hardening materials, it is assumed that the volume of the material displaced by the indenter is accommodated by the radial expansion of the hemispherical core, as was done in Johnson (1970). For conical indenters (see Fig. 1(a)), this volume conservation gives

$$\pi a^2 \cot\alpha \, \mathrm{d}a = 2\pi a^2 \, \mathrm{d}u|_{r=a}, \tag{11}$$

where a is the radius of the hemispherical hydrostatic core (which is also the radius of the projected area of the indentation), u is the radial displacement, α is the half included angle of the conical indenter (see Fig. 1(a)). For spherical indenters (see Fig. 1(b)), the assumed conservation of volume of the core yields

$$\pi a^2 \, \mathrm{d}h = 2\pi a^2 \, \mathrm{d}u|_{r=a}, \tag{12}$$

where h is the indentation depth satisfying $h = R - \sqrt{R^2 - a^2}$, with $R(>a)$ being the radius of the spherical indenter. Since the left-hand side of Eq. (12) represents the differentiation (increment) of the volume displaced by the indenter tip, which is a spherical cap in contact with the indented material, the fact that plastic deformation starts only at a finite value of a in a spherical indentation (e.g., Tabor, 1986), which differs from that in a conical indentation with a sharp indenter where plastic flow occurs instantaneously upon loading, has been automatically incorporated in Eq. (12) (and thus in the new ECM for spherical indentations).

From Eq. (4e) (or Eq. (8e)) it follows that the rate of change of the radial displacement at any r in the plastic zone (i.e., $a \leqslant r \leqslant r_c$ here) with respect to r_c is

$$\frac{du}{dr_c} = \frac{3}{2}\frac{\sigma_y}{E}\frac{r_c^2}{r^2}, \tag{13}$$

which gives

$$du|_{r=a} = \frac{3}{2}\frac{\sigma_y}{E}\frac{r_c^2}{a^2}\,dr_c. \tag{14}$$

Note that $r_i = a$ in the current application of the solutions presented in Section 2. The result given in Eq. (14) holds for both the elastic power-law hardening and the elastic linear-hardening materials, since the expression for the radial displacement u is the same in both cases, as noted earlier. Using Eq. (14) in Eq. (11) leads to, for *conical* indenters,

$$3r_c^2\,dr_c = \frac{E\cot\alpha}{\sigma_y}a^2\,da. \tag{15}$$

A direct integration of Eq. (15) yields, noting that $r_c \to 0$ as $a \to 0$ (i.e., no indentation deformation),

$$\left(\frac{r_c}{a}\right)^3 = \frac{1}{3}\frac{E}{\sigma_y}\cot\alpha. \tag{16}$$

Substituting Eq. (16) into Eq. (7), with p_i there replaced now by p, leads to

$$\frac{p}{\sigma_y} = \frac{2}{3}\left\{1 + \frac{1}{n}\left[\left(\frac{1}{3}\frac{E}{\sigma_y}\cot\alpha\right)^n - 1\right]\right\} \tag{17}$$

for *elastic power-law hardening* materials, and inserting Eq. (16) into Eq. (10) gives

$$\frac{p}{\sigma_y} = \frac{2}{3}\left[1 + \frac{E_p}{E}\left(\frac{1}{3}\frac{E}{\sigma_y}\cot\alpha - 1\right) + \left(1 - \frac{E_p}{E}\right)\ln\left(\frac{1}{3}\frac{E}{\sigma_y}\cot\alpha\right)\right] \tag{18}$$

for *elastic linear-hardening* materials. Note that p in Eqs. (17) and (18) is the hydrostatic pressure satisfying $\sigma_{rr}|_{r=a} = -p$ and represents, in an approximate manner, the mean contact pressure (i.e., applied load/projected area of the indentation $= P/(\pi a^2)$), thereby measuring the hardness (H) of the indented material (i.e., $p = H$) (Tabor, 1986). When $n \to 0$, i.e., for elastic-perfectly plastic materials, Eq. (17) reduces to, with the use of l'Hôpital's rule,

$$\frac{p}{\sigma_y} = \frac{2}{3}\left[1 + \ln\left(\frac{1}{3}\frac{E}{\sigma_y}\cot\alpha\right)\right]. \tag{19}$$

Also, when $E_p = 0$, i.e., for elastic-perfectly plastic materials, Eq. (18) reduces to Eq. (19). Eq. (19) is the same as that obtained by Johnson (1970) (see Eq. (1)) for *conical* indentations of incompressible *elastic-perfectly plastic* materials, thereby verifying the newly derived ECM models for conical indentations. Clearly, Eqs. (17)–(19) show that the indentation hardness H ($=p$) is independent of the indentation size a (and any other length parameter), indicating that the indentation process by a conical indenter is geometrically self-similar. This self-similarity unique to conical (and pyramidal) indenters is also known to exist for elastic solids (e.g., Tabor, 1986). However, the dependence of the indentation hardness on the shape of the indenter, as reflected through α, can be readily seen from Eqs. (17)–(19) for both elastic-perfectly plastic and elastic strain-hardening materials. This dependence of hardness on the indenter cone angle has also been demonstrated experimentally (e.g., Atkins and Tabor, 1965) and computationally (e.g., Cheng and Li, 2000), which implies that indentation hardness is not an absolute material property and therefore the cone angle associated with its determination needs to be specified.

Similarly, using Eq. (14) in Eq. (12) yields, for *spherical* indenters,

$$3r_c^2 \mathrm{d}r_c = \frac{E}{\sigma_y}\frac{1}{R}a^3\,\mathrm{d}a, \tag{20}$$

where use has been made of Taylor's expansion:

$$\mathrm{d}h = \frac{a\,\mathrm{d}a}{\sqrt{R^2-a^2}} = \frac{a}{R}\,\mathrm{d}a\left(1+\frac{1}{2}\frac{a^2}{R^2}+\cdots\right), \tag{21}$$

with all non-linear terms truncated. This approximation should work well for spherical indentations with small a/R (and therefore small indentation depth h). A direct integration of Eq. (20) yields, noting that $r_c \to 0$ as $a \to 0$,

$$\left(\frac{r_c}{a}\right)^3 = \frac{1}{4}\frac{E}{\sigma_y}\frac{a}{R}. \tag{22}$$

Substituting Eq. (22) into Eq. (7) then leads to

$$\frac{p}{\sigma_y} = \frac{2}{3}\left\{1+\frac{1}{n}\left[\left(\frac{1}{4}\frac{E}{\sigma_y}\frac{a}{R}\right)^n - 1\right]\right\} \tag{23}$$

for *elastic power-law hardening* materials, and inserting Eq. (22) into Eq. (10) gives

$$\frac{p}{\sigma_y} = \frac{2}{3}\left[1+\frac{E_p}{E}\left(\frac{1}{4}\frac{E}{\sigma_y}\frac{a}{R}-1\right)+\left(1-\frac{E_p}{E}\right)\ln\left(\frac{1}{4}\frac{E}{\sigma_y}\frac{a}{R}\right)\right] \tag{24}$$

for *elastic linear-hardening* materials. For elastic-perfectly plastic materials, both Eqs. (23) and (24) reduce to, by letting $n \to 0$ and $E_p = 0$ respectively,

$$\frac{p}{\sigma_y} = \frac{2}{3}\left[1+\ln\left(\frac{1}{4}\frac{E}{\sigma_y}\frac{a}{R}\right)\right] \tag{25}$$

for *spherical* indentations. From Eqs. (23)–(25) it is clear that the hardness $H(=p)$ now depends on the indentation size a and the radius of the indenter R, implying that the indentation process by a spherical indenter (with fixed R and changing a) is not self-similar even in the context of the linearized analysis presented here. Again, for elastic solids the dependence of hardness on R has been analytically shown (e.g., Tabor, 1986). This dependence of indentation hardness on indenter geometry exhibited by spherical indentations of both elastic and elastic–plastic materials supplements what is observed for conical indentations discussed above and, once again, indicates that indentation hardness, defined as the ratio of applied load to projected area of the indentation, is not an absolute material property.

Eqs. (17) and (23) represent an expanding cavity model (ECM) for *elastic power-law hardening* materials, whereas Eqs. (18) and (24) constitute a second ECM for *elastic linear-hardening* materials. Clearly, Eqs. (17), (18), (23) and (24) show that for a given indenter geometry the indentation hardness depends on E, σ_y and n or E_p. These two ECMs can be utilized to estimate the hardness of a material with strain-hardening characteristics, which supplement the existing ECM for *elastic-perfectly plastic* materials developed by Johnson (1970).

On the other hand, Johnson's ECM in its original form is known to predict lower hardness values than experimentally measured ones (e.g., Studman et al., 1977). As a result, attempts have been made to modify the original ECM of Johnson (1970). One modification was suggested by Johnson himself (Johnson, 1985)

through adding $2\sigma_y/3$ to the indentation pressure $p(=H)$. However, no detail was provided in Johnson (1985) regarding how the correction term was mathematically obtained, which makes it difficult for one to extend Johnson's modification for elastic-perfectly plastic materials to elastic strain-hardening materials. In comparison, the modification by Studman et al. (1977), which considers the variations in the stresses in the hemispherical core beneath the indenter from hydrostatic to other values that obey the von Mises yield condition, appears to be detailed, simple and also leads to better predictions (i.e., closer to the experimental data) than the original ECM of Johnson does. This modification, being also approximate (and thus non-unique), was motivated by the need to better correlate the predicted hardness values with experimentally measured ones and was based on the observation that there exists a jump (step-discontinuity) in $\sigma_e(=\sigma_{\theta\theta}-\sigma_{rr})$ from $r=a^-$, where $\sigma_e=0$ due to the assumed hydrostatic stress state with $\sigma_{\theta\theta}=\sigma_{rr}=\sigma_{\varphi\varphi}=-p$, to $r=a^+$ where $\sigma_e=\sigma_y$ for elastic-perfectly plastic materials. Hence, the idea used in Studman et al. (1977) to improve Johnson's ECM for elastic-perfectly plastic materials is adopted to modify the two ECMs for elastic strain-hardening materials developed above. The modification procedure follows that used in Studman et al. (1977) and is therefore excluded here. The major difference is that σ_y in the von Mises yield condition $|\sigma_{\theta\theta}|_{r=a}-\sigma_{rr}|_{r=a}|=\sigma_y$ used there is now replaced by $\sigma_e|_{r=a}$ (i.e., the effective stress on the interface $r=a$). Owing to the strain-hardening effect, there is $\sigma_e|_{r=a}\geqslant\sigma_y$, where the equality holds only when $r_c=a$. The results after the modification are listed below.

For *elastic power-law hardening* materials, the modified formulas are

$$\frac{H}{\sigma_y}=\frac{2}{3}\left\{\left(1-\frac{1}{n}\right)+\left(\frac{3}{4}+\frac{1}{n}\right)\left(\frac{1}{3}\frac{E}{\sigma_y}\cot\alpha\right)^n\right\} \tag{26}$$

for *conical* indentations, and

$$\frac{H}{\sigma_y}=\frac{2}{3}\left\{\left(1-\frac{1}{n}\right)+\left(\frac{3}{4}+\frac{1}{n}\right)\left(\frac{1}{4}\frac{E}{\sigma_y}\frac{a}{R}\right)^n\right\} \tag{27}$$

for *spherical* indentations. Eqs. (26) and (27) are obtained from modifying Eqs. (17) and (23), respectively.

For *elastic linear-hardening* materials, the modified formulas are

$$\frac{H}{\sigma_y}=\frac{2}{3}\left[\frac{7}{4}+\frac{7}{4}\frac{E_p}{E}\left(\frac{1}{3}\frac{E}{\sigma_y}\cot\alpha-1\right)+\left(1-\frac{E_p}{E}\right)\ln\left(\frac{1}{3}\frac{E}{\sigma_y}\cot\alpha\right)\right] \tag{28}$$

for *conical* indentations, and

$$\frac{H}{\sigma_y}=\frac{2}{3}\left[\frac{7}{4}+\frac{7}{4}\frac{E_p}{E}\left(\frac{1}{4}\frac{E}{\sigma_y}\frac{a}{R}-1\right)+\left(1-\frac{E_p}{E}\right)\ln\left(\frac{1}{4}\frac{E}{\sigma_y}\frac{a}{R}\right)\right] \tag{29}$$

for *spherical* indentations. Eqs. (28) and (29) are obtained from modifying Eqs. (18) and (24), respectively.

For *elastic-perfectly plastic* materials, both Eqs. (26) and (28) reduce to, by letting $n\to 0$ and $E_p=0$ respectively,

$$\frac{H}{\sigma_y}=\frac{2}{3}\left[\frac{7}{4}+\ln\left(\frac{1}{3}\frac{E}{\sigma_y}\cot\alpha\right)\right] \tag{30}$$

for *conical* indentations, and both Eqs. (27) and (29) reduce to, by letting $n\to 0$ and $E_p=0$ respectively,

$$\frac{H}{\sigma_y}=\frac{2}{3}\left[\frac{7}{4}+\ln\left(\frac{1}{4}\frac{E}{\sigma_y}\frac{a}{R}\right)\right] \tag{31}$$

for *spherical* indentations. Eq. (30) is the same as that given in Studman et al. (1977) (see Eq. (13) there) for *conical* indentations of elastic-perfectly plastic materials, thereby verifying the modified ECM models for strain-hardening materials obtained here in Eqs. (26)–(29). These newly derived formulas will be applied in the next section to analyze sample cases.

4. Numerical results

To illustrate the two ECMs derived in the preceding section, a parametric study has been conducted by directly using Eqs. (26) and (28) for conical indentations and Eqs. (27) and (29) for spherical indentations of elastic strain-hardening materials. The numerical results are presented below in this section.

Fig. 2 shows how the hardness (H) of an elastic power-law hardening material changes with n and E when a conical indenter with $\alpha = 70.3°$ is employed, while Fig. 3 illustrates how the hardness of an elastic linear-hardening material varies with E_p and E when the same conical indenter is used. The numerical values of the former are based on Eq. (26), whereas those of the latter on Eq. (28). It is observed from Figs. 2 and 3 that the increase of H with E exhibited by the elastic-perfectly plastic material (i.e., the solid lines with $n = 0$ or $E_p/E = 0$), as predicted by the modified ECM model given in Studman et al. (1977) (see Eq. (30)), is also demonstrated by both the elastic power-law hardening and the elastic linear-hardening materials, as predicted by the two newly developed models. In addition, H is seen to increase as n or E_p increases. That is, the higher the strain-hardening level is, the larger the hardness is.

The effects of α on H, as predicted by the two new models for conical indentations, are shown, respectively, in Figs. 4 and 5 for the elastic power-law hardening material and the elastic linear-hardening

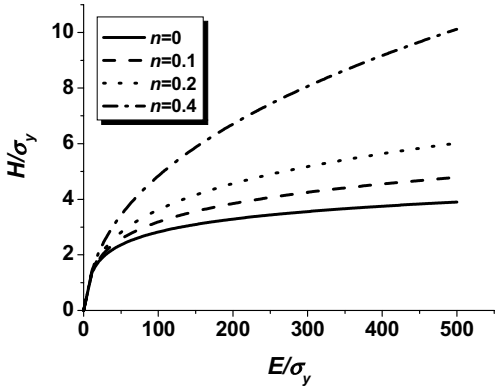

Fig. 2. The influence of n on H for a conical indenter with $\alpha = 70.3°$.

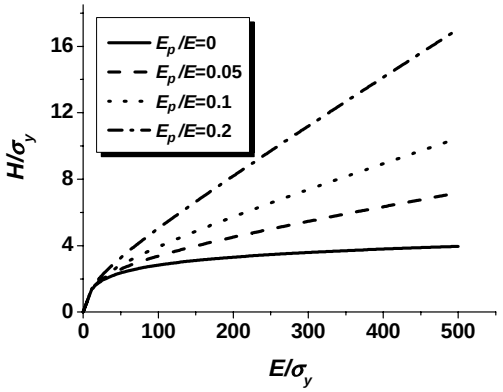

Fig. 3. The influence of E_p on H for a conical indenter with $\alpha = 70.3°$.

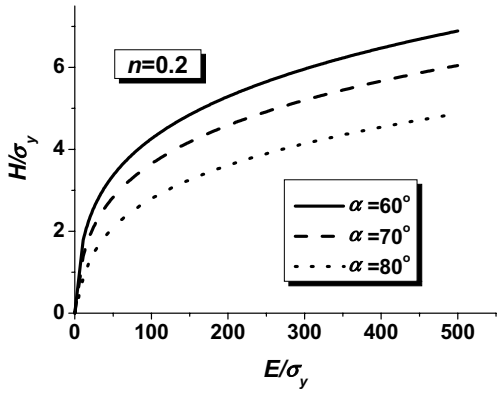

Fig. 4. The effect of α on H for the elastic power-law hardening material (with $n = 0.2$).

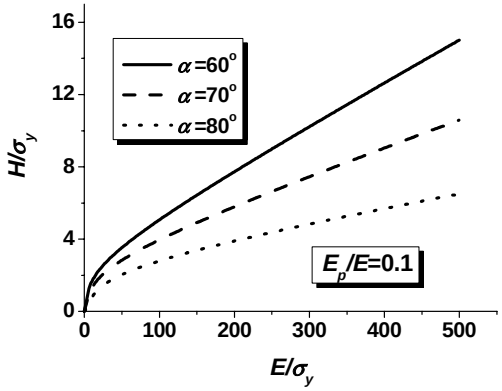

Fig. 5. The effect of α on H for the elastic linear-hardening material (with $E_p/E = 0.1$).

material. For both types of the strain-hardening materials, it is seen that the use of a conical indenter with smaller values of α (i.e., a sharper indenter) leads to larger values of H. For example, when $E/\sigma_y = 100$, H/σ_y decreases from 4.3 to 2.8 for the power-law hardening material (with $n = 0.2$) and from 5.1 to 2.8 for the linear-hardening material (with $E_p/E = 0.1$) as α changes from 60° to 80°. This quantitatively shows that the indentation hardness is indeed strongly dependent on the cone angle α, as was revealed experimentally by Atkins and Tabor (1965) and computationally by Cheng and Li (2000).

Figs. 6 and 7 illustrate how H varies with a/R for spherical indentations of elastic power-law hardening and elastic linear-hardening materials, respectively. The numerical results shown in these two figures are based on Eqs. (27) and (29). From Figs. 6(a,b) and 7(a,b) it is seen that when the indented material is soft (with $E/\sigma_y \leqslant 100$, i.e., a large value of σ_y) and the indentation depth is small (with $a/R < 0.1$, i.e., a small value of a), the hardness is insignificantly affected by the strain-hardening behavior. This is due to the dominance of the Hertzian elastic contact, since the finite value of a required for initiating plastic deformations under the given conditions, as noted earlier (near Eq. (2)), may not have been reached. However, when the indented material is stiff (with $E/\sigma_y > 100$, i.e., a small value of σ_y) and/or the indentation depth is large (i.e., with a large value of a), plastic deformations become significant and the strain-hardening behavior of the material has a large effect on the hardness, as shown in Figs. 6 and 7.

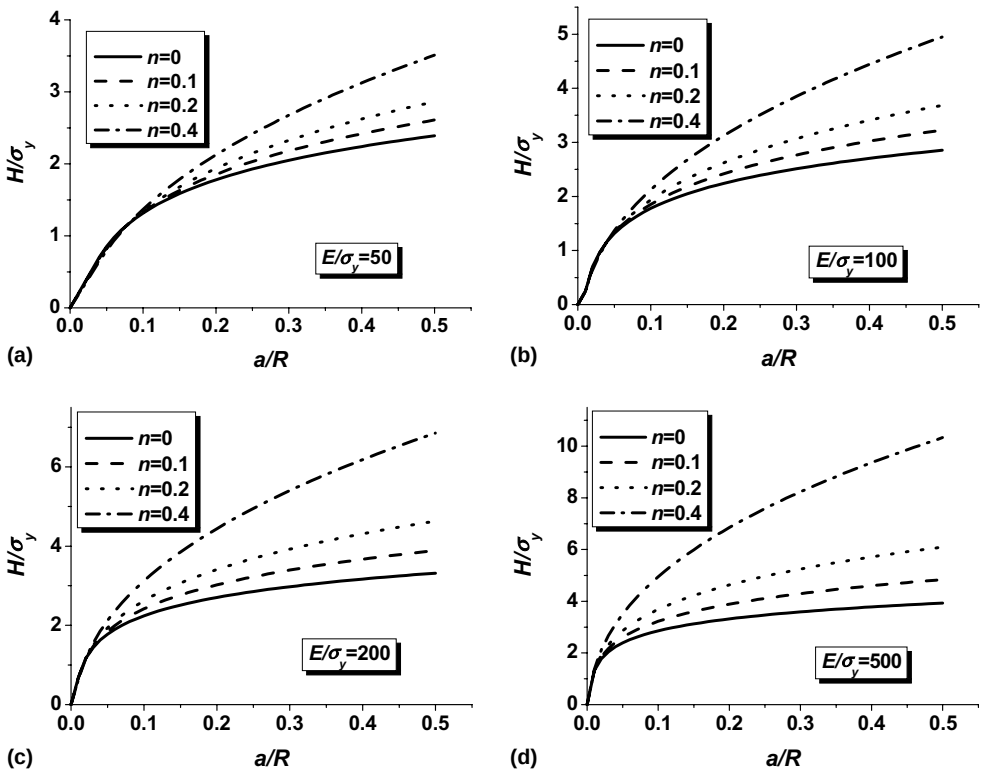

Fig. 6. The effect of n on H for spherical indentations of elastic power-law hardening materials.

The variations of H with E for both the elastic power-law hardening and the elastic linear-hardening materials in spherical indentations are illustrated in Fig. 8. It is observed from Fig. 8 that for all of the spherical indentations (with different values of a/R) considered the higher E is, the larger H is.

Clearly, Figs. 6–8 quantitatively show that the indentation hardness H strongly depends on the spherical indenter geometry through a/R, which is also revealed by the finite element results of Park and Pharr (2004).

A comparison between the newly developed analytical model and the finite element (FE) simulation of Park and Pharr (2004) for spherical indentations of elastic power-law hardening materials is shown in Fig. 9, where $E^* \equiv E/(1-\nu^2)$. As illustrated in Fig. 9, when the indentation depth is small (with $E^*a/(\sigma_y R) < 10$, i.e., a small value of a and/or a large value of σ_y), the hardness, according to the new model (see Eq. (27)), does not appear to vary with the strain-hardening exponent n, which is also revealed by the FE results of Park and Pharr (2004). The reason for this is that the small plastic deformation zone induced by the small-depth indentation with the value of a above but close to the required critical value for initiating plastic deformations is constrained by the surrounding material undergoing elastic deformations, as was also observed by Park and Pharr (2004). When the indentation depth (and thus the value of a) is large (i.e., with extensive plastic deformations), however, the hardness predicted by the new model depends strongly on n, as shown in Figs. 6 and 9. Also, it can be seen from Fig. 9 that when the material is stiff enough (with $E^*a/(\sigma_y R) > 20$) the agreement between the new model and the FE model is fairly good, while for the material with $E^*a/(\sigma_y R) < 20$ a sizable discrepancy exists between the two models. This deviation is believed to arise mainly from two factors: one is the assumed incompressibility (i.e., Poisson' ratio $\nu = 0.5$) in the new model,

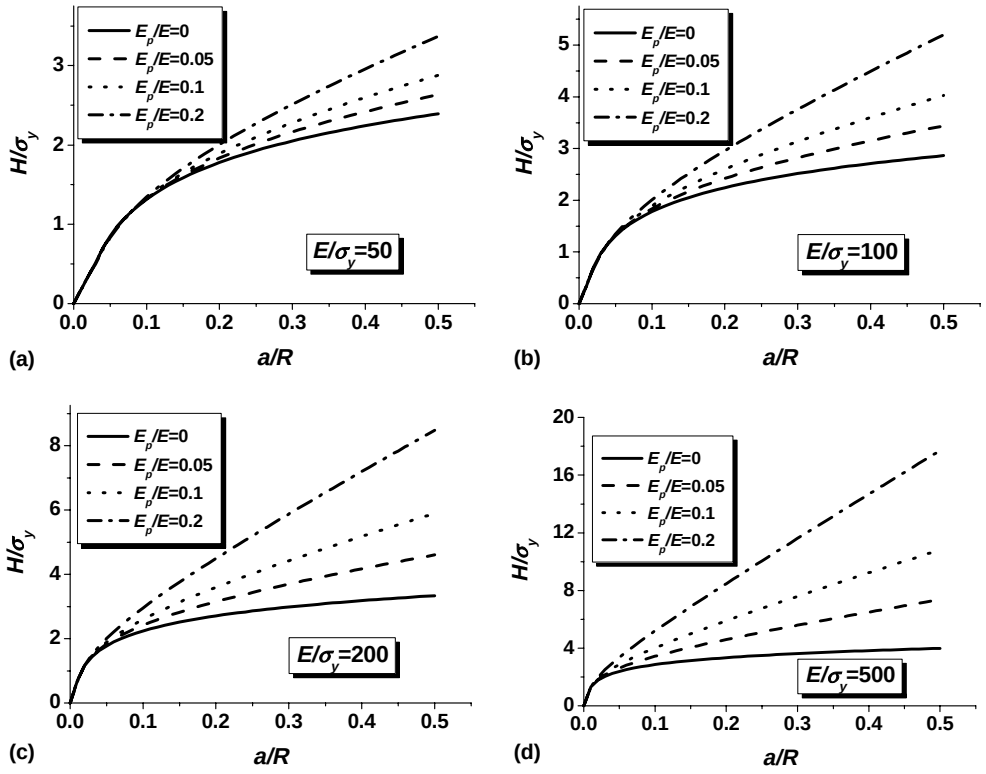

Fig. 7. The effect of E_p on H for spherical indentations of elastic linear-hardening materials.

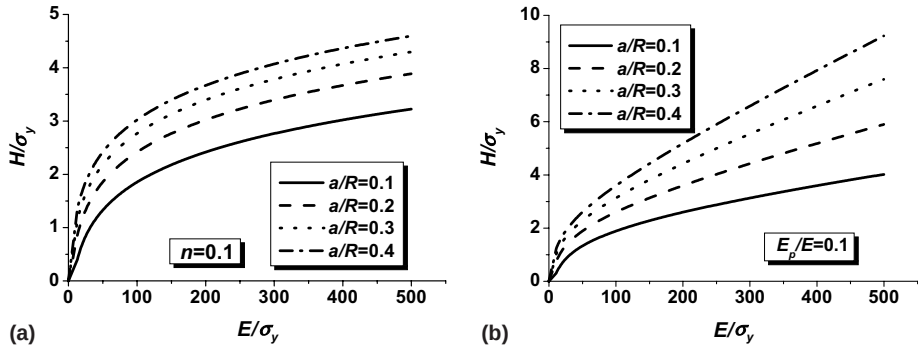

Fig. 8. Variation of H with E for spherical indentations with different a/R: (a) elastic power-law hardening material with $n = 0.1$; (b) elastic linear-hardening material with $E_p/E = 0.1$.

as opposed to the compressibility (with $v = 0.3$) used in Park and Pharr (2004); the other is the use of a finite cylinder with traction-free and zero-displacement boundary conditions to represent the indented material in the FE model of Park and Pharr (2004), compared with the infinite half-space with the top surface being not traction-free involved in developing the ECM. Nevertheless, the trends predicted by the new analytical model are seen to agree with those by the FE model of Park and Pharr (2004), thereby supporting the new model.

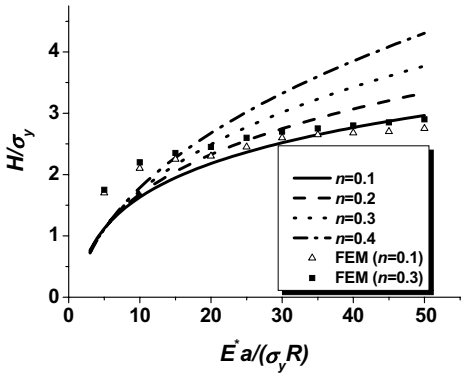

Fig. 9. Comparison with the FEM results of Park and Pharr (2004) for spherical indentations of elastic power-law hardening materials.

5. Summary

Two expanding cavity models (ECMs)—one for elastic power-law hardening materials and the other for elastic linear-hardening materials—are developed using two elastic–plastic solutions for internally pressurized thick-walled spherical shells of strain-hardening materials. Both conical and spherical indentations are considered in the formulation. The closed-form formulas derived show that for a given indenter geometry indentation hardness depends on Young's modulus, yield stress and strain-hardening index of the indented material. It is seen that the two new models reduce to Johnson's ECM for elastic-perfectly plastic materials when there is no strain-hardening.

To illustrate the two newly developed models, a parametric study is conducted. The numerical results reveal that the hardness of the indented material increases with the Young's modulus and strain-hardening level of the material. It is also found that for conical indentations the hardness depends on the sharpness of the conical indenter: the sharper the indenter is, the larger the hardness is. For spherical indentations the indentation hardness is seen to be significantly affected by the strain-hardening level when the indented material is stiff (i.e., with a large ratio of Young's modulus to yield stress) and/or the indentation depth is large. When the indentation depth is small (i.e., there is little or no plastic deformation induced by the spherical indenter), the hardness appears to be independent of the strain-hardening level, which agrees with what was shown by the FE results of Park and Pharr (2004).

Acknowledgements

The work reported here was funded by a grant from the U.S. NSF (grant # CMS-0324461), with Dr. Ken Chong as the program manager. This support is gratefully acknowledged. The authors also wish to thank the two anonymous reviewers for their helpful comments on an earlier version of the paper.

Appendix A

The solution for an internally pressurized spherical shell of the elastic linear-hardening material defined in Eq. (3) is derived here. The derivation follows the procedure used in Gao and Wei (1991) (see also Gao, 2003) for the spherical shell of the elastic power-law hardening material defined in Eq. (2).

Based on the assumptions of material incompressibility and small deformations, the governing equations in the plastic region of the shell wall ($r_i \leqslant r \leqslant r_c$), which incorporate Hencky's deformation theory and von Mises' yield criterion, include (Gao and Wei, 1991; Gao, 1994), in a stress formulation,

$$\sigma_{\theta\theta} - \sigma_{rr} = \frac{1}{2} r \frac{d\sigma_{rr}}{dr}, \tag{A.1}$$

$$\sigma_e = \sigma_y + E_p(\varepsilon_e - \varepsilon_y), \tag{A.2}$$

$$\varepsilon_{\theta\theta} = \varepsilon_{\varphi\varphi} = \frac{1}{2}\frac{\varepsilon_e}{\sigma_e}(\sigma_{\theta\theta} - \sigma_{rr}), \quad \varepsilon_{rr} = -\frac{\varepsilon_e}{\sigma_e}(\sigma_{\theta\theta} - \sigma_{rr}), \tag{A.3}$$

$$\sigma_e = \sigma_{\theta\theta} - \sigma_{rr}, \tag{A.4}$$

$$r\frac{d\varepsilon_{\theta\theta}}{dr} = \varepsilon_{rr} - \varepsilon_{\theta\theta}. \tag{A.5}$$

The boundary conditions are

$$\sigma_{rr}|_{r=r_i} = -p_i, \quad \sigma_{rr}|_{r=r_c} = -p_c, \quad \sigma_e|_{r=r_c} = \sigma_y. \tag{A.6a, b, c}$$

Eqs. (A.1)–(A.6a,b,c) define the boundary-value problem (BVP) for determining the stress and strain components in the plastic region ($r_i \leqslant r \leqslant r_c$). This BVP can be solved as follows.

Using Eq. (A.4) in Eq. (A.3) gives

$$\varepsilon_{\theta\theta} = \varepsilon_{\varphi\varphi} = \frac{1}{2}\varepsilon_e, \quad \varepsilon_{rr} = -\varepsilon_e. \tag{A.7}$$

Inserting Eq. (A.7) into Eq. (A.5) then results in

$$\frac{d\varepsilon_e}{\varepsilon_e} = -3\frac{dr}{r}, \tag{A.8}$$

which can be integrated to obtain

$$\varepsilon_e = \frac{c}{r^3}, \tag{A.9}$$

where c is an integration constant. Substituting Eq. (A.9) into Eq. (A.2) yields

$$\sigma_e = \sigma_y + E_p\left(\frac{c}{r^3} - \varepsilon_y\right). \tag{A.10}$$

The use of Eq. (A.10) in Eq. (A.6c) leads to

$$c = \frac{\sigma_y}{E} r_c^3. \tag{A.11}$$

Inserting Eqs. (A.10), (A.11) and (A.4) into Eq. (A.1) then gives

$$d\sigma_{rr} = 2\sigma_y\left[1 + \frac{E_p}{E}\left(\frac{r_c^3}{r^3} - 1\right)\right]\frac{dr}{r}. \tag{A.12}$$

Integrating Eq. (A.12) with respect to r from r_c to r results in, with the use of Eq. (A.6b),

$$\sigma_{rr} = -p_c + 2\sigma_y\left(1 - \frac{E_p}{E}\right)\ln\frac{r}{r_c} + \frac{2\sigma_y}{3}\frac{E_p}{E}\left(1 - \frac{r_c^3}{r^3}\right), \tag{A.13}$$

where p_c, as first introduced in Eq. (A.6b), is the pressure acting on the elastic–plastic interface $r = r_c$. The relation between p_c and r_c is to be determined from the solution in the elastic region (see Gao and Wei, 1991).

The stress components in the elastic region of the shell wall ($r_c \leqslant r \leqslant r_o$), which can be reviewed as a thick-walled spherical shell of the inner radius r_c and the outer radius r_o subjected to the internal pressure p_c, are given by Lamé's solution listed in Eq. (6a,b) (e.g., Gao and Wei, 1991). Hence, using Eqs. (6b), (A.4) and (A.6b) in Eq. (A.6c) yields

$$p_c = \frac{2\sigma_y}{3}\left(1 - \frac{r_c^3}{r_o^3}\right). \tag{A.14}$$

Substituting Eq. (A.14) into Eq. (A.13) gives

$$\sigma_{rr} = 2\sigma_y\left(1 - \frac{E_p}{E}\right)\ln\frac{r}{r_c} + \frac{2\sigma_y}{3}\frac{E_p}{E}\left(1 - \frac{r_c^3}{r^3}\right) - \frac{2\sigma_y}{3}\left(1 - \frac{r_c^3}{r_o^3}\right). \tag{A.15}$$

The use of Eq. (A.15) in Eq. (A.1) leads to

$$\sigma_{\theta\theta} = 2\sigma_y\left(1 - \frac{E_p}{E}\right)\ln\frac{r}{r_c} - \frac{\sigma_y}{3}\frac{E_p}{E}\left(1 - \frac{r_c^3}{r^3}\right) + \frac{\sigma_y}{3}\left(1 + \frac{2r_c^3}{r_o^3}\right) = \sigma_{\varphi\varphi}. \tag{A.16}$$

Using Eq. (A.15) in Eq. (A.6a), which is the only remaining boundary condition, results in

$$\frac{p_i}{\sigma_y} = \frac{2}{3}\left[\left(1 - \frac{r_c^3}{r_o^3}\right) - \frac{E_p}{E}\left(1 - \frac{r_c^3}{r_i^3}\right)\right] + 2\left(1 - \frac{E_p}{E}\right)\ln\frac{r_c}{r_i}, \tag{A.17}$$

which will be solved numerically to obtain r_c for given loading (p_i), material properties (E, E_p, σ_y) and shell geometry (r_i, r_o).

Next, substituting Eqs. (A.9) and (A.11) into Eq. (A.7) gives the strain components as

$$\varepsilon_{\theta\theta} = \varepsilon_{\varphi\varphi} = \frac{1}{2}\frac{\sigma_y}{E}\frac{r_c^3}{r^3}, \quad \varepsilon_{rr} = -\frac{\sigma_y}{E}\frac{r_c^3}{r^3}. \tag{A.18}$$

Then, using the geometrical equations given by

$$\varepsilon_{\theta\theta} = \varepsilon_{\varphi\varphi} = \frac{u}{r}, \quad \varepsilon_{rr} = \frac{\mathrm{d}u}{\mathrm{d}r}, \tag{A.19}$$

the only non-zero (radial) displacement, u, will be readily obtained from Eqs. (A.18) and (A.19) as

$$u = \frac{\sigma_y}{2E}\frac{r_c^3}{r^2}. \tag{A.20}$$

Eqs. (A.15)–(A.18) and (A.20) provide the complete solution for the plastic region ($r_i \leqslant r \leqslant r_c$) in the wall of the spherical shell, which are listed in Eqs. (8a–e) and 9.

It should be pointed out that a solution for the same problem was furnished, without detailed derivations, in Mendelson (1968) by regarding the material as compressible. When Poisson's ratio equals 0.5, that solution recovers Eqs. (A.15) and (A.17), but it cannot recover Eq. (A.16). This necessitates the inclusion of the detailed derivation of the present solution here.

References

Atkins, A.G., Tabor, D., 1965. Plastic indentation in metals with cones. J. Mech. Phys. Solids 13, 149–164.
Cheng, Y.-T., Cheng, C.-M., 2004. Scaling, dimensional analysis, and indentation measurements. Mater. Sci. Eng. R 44, 91–149.
Cheng, Y.-T., Li, Z., 2000. Hardness obtained from conical indentations with various cone angles. J. Mater. Res. 15, 2830–2835.
Fischer-Cripps, A.C., 1997. Elastic–plastic behaviour in materials loaded with a spherical indenter. J. Mater. Sci. 32, 727–736.
Fischer-Cripps, A.C., 2002. Nanoindentation. Springer, New York.
Gao, X.-L., 1992. An exact elasto-plastic solution for an open-ended thick-walled cylinder of a strain-hardening material. Int. J. Pres. Ves. Piping 52, 129–144.

Gao, X.-L., 1993. An exact elasto-plastic solution for a closed-end thick-walled cylinder of elastic linear-hardening material with large strains. Int. J. Pres. Ves. Piping 56, 331–350.

Gao, X.-L., 1994. An exact elasto-plastic solution for a thick-walled spherical shell of elastic linear-hardening material with finite deformations. Int. J. Pres. Ves. Piping 57, 45–56.

Gao, X.-L., 2003. Strain gradient plasticity solution for an internally pressurized thick-walled spherical shell of an elastic–plastic material. Mech. Res. Comm. 30, 411–420.

Gao, X.-L., Wei, X.-X., 1991. An exact elasto-plastic solution for a thick-walled spherical shell of a strain-hardening material. In: Brooks, G.N. et al. (Eds.), Pressure Vessels and Components-1991, PVP-vol. 217. ASME Press, New York, pp. 75–79.

Giannakopoulos, A.E., Suresh, S., 1999. Determination of elastoplastic properties by instrumented sharp indentation. Scripta Mater. 40, 1191–1198.

Hill, R., 1950. The Mathematical Theory of Plasticity. Oxford University Press, London.

Hirst, W., Howse, M.G.J.W., 1969. The indentation of materials by wedges. Proc. R. Soc. Lond. A311, 429–444.

Johnson, K.L., 1970. The correlation of indentation experiments. J. Mech. Phys. Solids 18, 115–126.

Johnson, K.L., 1985. Contact Mechanics. Cambridge University Press, Cambridge, p. 175.

Lawn, B.R., 1998. Indentation of ceramics with spheres: A century after Hertz. J. Amer. Ceram. Soc. 81, 115–126.

Marsh, D.M., 1964. Plastic flow in glass. Proc. R. Soc. Lond. A 279, 420–435.

Mata, M., Alcala, J., 2003. Mechanical property evaluation through sharp indentations in elastoplastic and fully plastic contact regimes. J. Mater. Res. 18, 1705–1709.

Mata, M., Anglada, M., Alcala, J., 2002. A hardness equation for sharp indentation of elastic-power-law strain-hardening materials. Philos. Mag. A82, 1831–1839.

Mendelson, A., 1968. Plasticity: Theory and Application. Macmillan, New York.

Mesarovic, S.D., Fleck, N.A., 1999. Spherical indentation of elastic–plastic solids. Proc. R. Soc. Lond. A 455, 2707–2728.

Narasimhan, R., 2004. Analysis of indentation of pressure sensitive plastic solids using the expanding cavity model. Mech. Mater. 36, 633–645.

Park, Y.J., Pharr, G.M., 2004. Nanoindentation with spherical indenters: Finite element studies of deformation in the elastic–plastic transition regime. Thin Solid Films 447–448, 246–250.

Studman, C.J., Moore, M.A., Jones, S.E., 1977. On the correlation of indentation experiments. J. Phys. D: Appl. Phys. 10, 949–956.

Tabor, D., 1951. Hardness of Metals. Clarendon Press, Oxford.

Tabor, D., 1986. Indentation hardness and its measurement: some cautionary comments. In: Blau, P.J., Lawn, B.R. (Eds.), Microindentation Techniques in Materials Science and Engineering, ASTM STP 889. ASTM Press, Philadelphia, pp. 129–159.

Wei, Y., Hutchinson, J.W., 2003. Hardness trends in micron scale indentation. J. Mech. Phys. Solids 51, 2037–2056.

Zhang, W., Subhash, G., 2001. An elastic–plastic-cracking model for finite element analysis of indentation cracking in brittle materials. Int. J. Solids Struct. 38, 5893–5913.